Hindawi
Advances in Civil Engineering
Volume 2020, Article ID 7560219, 10 pages
https://doi.org/10.1155/2020/7560219

Research Article

3D Limit Analysis of the Transient Stability of Slope during Pile Driving in Nonhomogeneous and Anisotropic Soil

Pingping Rao,[1,2] **Jian Wu**,[2] **and Zhihao Mo**[2]

[1]*School of Civil Engineering, Kashgar University, Kashgar, Xinjiang Uygur Autonomous Region, 844000, China*
[2]*Department of Civil Engineering, University of Shanghai for Science and Technology, Shanghai 200093, China*

Correspondence should be addressed to Pingping Rao; raopingping@usst.edu.cn

Received 19 December 2019; Revised 21 March 2020; Accepted 21 May 2020; Published 9 June 2020

Academic Editor: Kirk Hatfield

To evaluate the stability of a slope subjected to pile driving in nonhomogeneous and anisotropic soils, an upper-bound limit analysis method is employed in this paper. A 3D rotational failure mechanism for soil slope is extended to account for different failure patterns (i.e., toe failure and base failure). In order to avoid missing the global minimum, an efficient optimization method is simultaneously employed to find the least upper bound to the factor of safety (F_S). The effectiveness and accuracy of the proposed method is well demonstrated by comparing the results obtained from the proposed approach with the solutions from published literatures. The effects of key designing parameters are presented and discussed. The optimal pile location and the three-dimensional effect of the slope are discussed. In addition, these results highlight that the adverse effects of pile driving on slope stability should be highly concerned during the design of geotechnical infrastructures, rather than emphasizing the reinforcement effect of a pile only.

1. Introduction

In geotechnical engineering, the stabilization of slopes by placing piles has been one of the most innovative and effective reinforcement techniques in recent years. All slope failures are 3D in nature, especially for the slopes with constraints on width. It is therefore much desirable to perform slope stability analysis in a 3D model, which is closer to the scenarios in engineering practice than a 2D model [1].

Current approaches for analyzing the stability of 3D slopes can be mainly divided into three categories: (1) traditional limit-equilibrium method, (2) numerical approaches, and (3) limit analysis. The most commonly used limit-equilibrium approach for 3D slope stability analysis is usually a direct extension from various 2D slice methods. Nevertheless, the majority of these studies are based on the assumptions relating to different internal force distributions, which are not easily justified [2–5]. Over the past decades, numerical approaches have also been widely used to estimate 3D slope stability. However, numerical analyses for 3D slope stability are often time-consuming, especially when the geology conditions are complex [6–10]. In contrast, due to the simplicity and efficiency, the limit analysis method (LAM) used in the 3D slope stability analysis has received increasing attention over recent decades [11–14]. The advantages of LAM mainly include that (i) it does not require any assumption of stresses on the failure surfaces and the critical failure surface can be determined automatically; (ii) this method only involves one unknown parameter (i.e., F_S). However, the majority of existing LAMs were limited to evaluate slopes without presence of piles. Reese [15] used the *p-y* method to extend the analysis of piles under lateral loading to the analysis of a single pile in rock and emphasized that the nonlinear behavior of piles must be considered. Conte et al. [16] adopted appropriate constitutive models that account for the nonlinearity of piles and soil to analyze the response of reinforced concrete flexible piles subjected to inclined loads based on the 3D finite element approach. However, these analyses are limited to homogeneous and isotropic soils, while soils are heterogeneous and anisotropic in nature.

This article presents a new method to estimate the F_S of 3D slopes by using the upper-bound limit analysis. Based on

the kinematic approach of limit analysis, the upper-bound expression for the F_S is defined as the ratio of the internal energy dissipation rate to the external work rate. The factor of safety is obtained by optimizing the variables of 3D mechanism. The numerical results of different parameters are calculated and listed in graphs, which can be used as a useful tool in practical applications. The accuracy and effectiveness of the method is demonstrated by comparing the results obtained by the proposed method with its counterparts obtained by Gao et al. [17] and Yang and Li [18]. In addition, the sensitivity of key designing parameters, e.g., cohesion, friction angle, inclined angle, pile location, maximum width of the 3D portion, heterogeneity, and anisotropy on the stability of earth slopes are presented and discussed.

2. Limit Analysis of 3D Nonhomogeneous and Anisotropic Slopes during Pile Driving

2.1. Force-Increase Technique. In slope stability analysis, the strength reduction method has been widely used to calculate the F_S [12, 19], where the F_S is defined as a critical reduction factor at which the shear strength of soil leads to the failure state of slopes. In addition to the strength reduction method, the force-increase technique has also been used for determining the F_S [20, 21] by gradually increasing the external forces until the failure of slope while the soil strength remains constant. The F_S is defined as the ratio of the increased external forces at failure to the initial external forces:

$$F_S = \frac{\gamma_{cr}}{\gamma} = \frac{q_{cr}}{q}, \tag{1}$$

where γ and q = initial unit weight of soil and surcharge, respectively, and γ_{cr} and q_{cr} = corresponding external forces at failure, respectively. Due to that the external work rate is a linear combination of external forces, the F_S is equivalent to the ratio of the work rate done by the critical external forces to the actual external work rate. As a result, the work rate which is due to the critical external forces takes the following form:

$$W_{cr} = W \cdot F_S, \tag{2}$$

where W = actual external work rate and W_{cr} = critical external work rate.

Based on the upper-bound limit analysis, equating the work rate of critical external forces W_{cr} to the rate of internal energy dissipation D and combining with equation (2) leads to the expression of the F_S as

$$F_S = \frac{D}{W}. \tag{3}$$

By employing the upper-bound limit analysis and force-increase technique, the F_S is defined as the ratio of the internal energy dissipation rate to the external work rate. It should be highlighted that the force-increase technique used herewith has an advantage over the strength reduction method when using three-dimensional mechanism to analyze slope stability. The force-increase technique can provide an explicit expression of the F_S, while the strength reduction method can only provide an implicit equation.

2.2. Failure Mechanism in Slopes. A slope as shown in Figure 1 is considered in this analysis. The surface of the slope is composed of the horizontal ground AB and the surface BC with inclined angle β. The height of the slope is H. X_f is the horizontal distance between the pile location and the slope toe. The 3D horn failure mechanism can be determined by two log spirals on the plane, which are AC,

$$r = r_0 e^{(\theta-\theta_0)\tan\varphi}, \tag{4}$$

$A'C'$, and

$$r' = r_0' e^{-(\theta-\theta_0)\tan\varphi}, \tag{5}$$

with $r_0 = OA$, $r_0' = OA'$, and θ_0 as illustrated in Figure 1. The 3D horn mechanism is generated by rotating a circle with an increasing diameter about the rotation center O. Thus, the failure mechanism has a shape of a curvilinear cone with apex angle 2φ, and all cross-sections are circular. The distance from the rotation center O to the circle center r_m and the radius R of a circle are given by

$$\begin{aligned} r_m &= \frac{r + r'}{2}, \\ R &= \frac{r - r'}{2}. \end{aligned} \tag{6}$$

As a result, the 3D failure mechanisms for slopes with finite width B modified with a plane insert with the width b could allow transition to the plane-strain mechanism as b approaches infinity (Figure 2). It is noted that similar concept has also been used in [22].

For 3D base-failure mechanism (Figures 1 and 2), the geometry of failure surface can be determined by the angle $\beta\prime$, as shown in Figure 1. The 3D toe-failure mechanism is a special case of the 3D base-failure mechanism when $\beta\prime$ equals the inclined angle β of slopes. However, the rate of work done and dissipated in the portion of a rotating block below the toe must be counted in the 3D base-failure mechanism. Following the procedure similar to Michalowski and Drescher [1] and Chen [22], the expressions of W and D for the 3D base-failure mechanism are derived as follows:

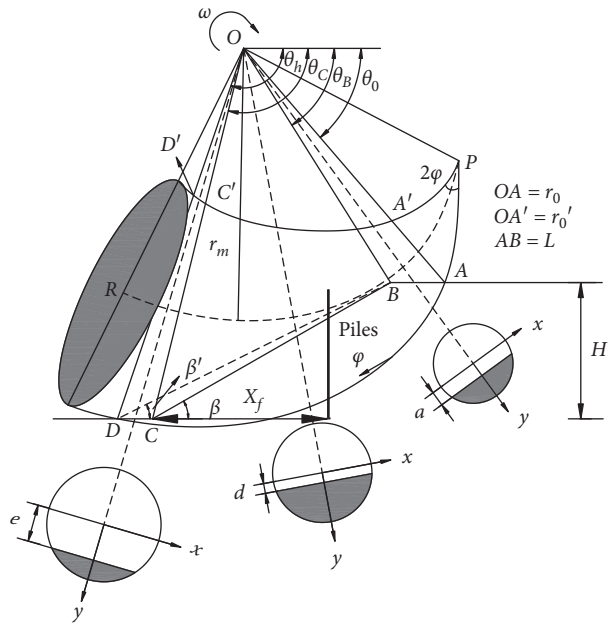

Figure 1: 3D rotational failure mechanism.

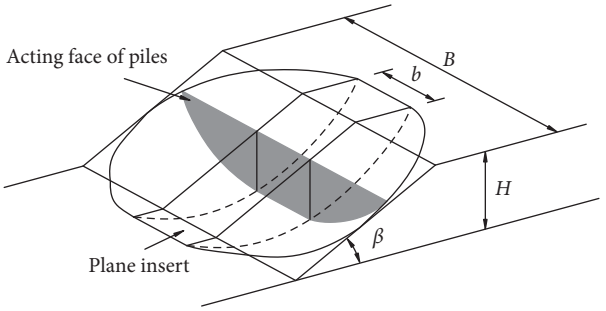

Figure 2: 3D failure mechanism with the plane insert.

(i) Gravity work of the insert block:

$$
\begin{aligned}
W_c &= b\gamma\omega r_0^3\left(f_1 - f_2 - f_3 - f_4\right),\\
f_1 &= \frac{1}{3\left(1+9\tan^2\varphi\right)}\left[\left(3\tan\varphi\cos\theta_h+\sin\theta_h\right)e^{3\left(\theta_h-\theta_0\right)\tan\varphi}-\left(3\tan\varphi\cos\theta_0+\sin\theta_0\right)\right],\\
f_2 &= \frac{1}{6}\frac{L}{r_0}\left(2\cos\theta_0-\frac{L}{r_0}\right)\sin\theta_0,\\
f_3 &= \frac{1}{6}e^{\left(\theta_h-\theta_0\right)\tan\varphi}\left[\sin\left(\theta_h-\theta_0\right)-\frac{L}{r_0}\sin\theta_h\right]\left[\cos\theta_0-\frac{L}{r_0}+\cos\theta_h e^{\left(\theta_h-\theta_0\right)\tan\varphi}\right],\\
f_4 &= \left(\frac{H}{r_0}\right)^2\frac{\sin\left(\beta-\beta\prime\right)}{2\sin\beta\sin\beta\prime}\left[\cos\theta_0-\frac{L}{r_0}-\frac{1}{3}\frac{H}{r_0}\left(\cot\beta\prime+\cot\beta\right)\right],\\
\frac{L}{r_0} &= \frac{\sin\left(\theta_0+\beta\prime\right)}{\sin\beta\prime}-\exp\left[\left(\theta_h-\theta_0\right)\tan\varphi\right]\frac{\sin\left(\theta_h+\beta\prime\right)}{\sin\beta\prime}.
\end{aligned}
\tag{7}
$$

(ii) Gravity work of the 3D spiral structure:

$$W_e = 2\omega\gamma\left[\int_{\theta_0}^{\theta_B}\int_0^{X_1}\int_{g_1}^{Y}(r_m+y)^2\cos\theta\,dx\,dy\,d\theta + \int_{\theta_B}^{\theta_C}\int_0^{X_2}\int_{g_2}^{Y}(r_m+y)^2\cos\theta\,dx\,dy\,d\theta + \int_{\theta_C}^{\theta_h}\int_0^{X_3}\int_{g_3}^{Y}(r_m+y)^2\cos\theta\,dx\,dy\,d\theta\right]. \quad (8)$$

(iii) Internal energy dissipation of the insert block:

$$D_c = b\omega\int_{\theta_0}^{\theta_h} c\,(r_m+R)^2 d\theta. \quad (9)$$

(iv) Internal energy dissipation of the 3D spiral structure:

$$D_e = 2\omega\left[\int_{\theta_0}^{\theta_B}\int_{g_1}^{R}\frac{(r_m+y)^2}{\sqrt{R^2-y^2}}cR\,dy\,d\theta + \int_{\theta_B}^{\theta_C}\int_{g_2}^{R}\frac{(r_m+y)^2}{\sqrt{R^2-y^2}}cR\,dy\,d\theta + \int_{\theta_C}^{\theta_h}\int_{g_3}^{R}\frac{(r_m+y)^2}{\sqrt{R^2-y^2}}cR\,dy\,d\theta\right], \quad (10)$$

where ω = the angular velocity, φ = the internal frictional angle, c = the cohesion, β = the slope angle, and H = the slope height, and θ_0, θ_B, θ_C, θ_h, and $\beta\prime$ are illustrated in Figure 1. Besides that,

$$\begin{aligned}
X_1 &= \sqrt{R^2-g_1^2},\\
X_2 &= \sqrt{R^2-g_2^2},\\
X_3 &= \sqrt{R^2-g_3^2},\\
Y &= \sqrt{R^2-x^2},\\
g_1 &= \frac{\sin\theta_0}{\sin\theta}r_0 - r_m,\\
g_2 &= \frac{\sin(\beta+\theta_h)}{\sin(\beta+\theta)}r_0 e^{(\theta_h-\theta_0)\tan\varphi} - r_m,\\
g_3 &= \frac{\sin\theta_h}{\sin\theta}r_0 e^{(\theta_h-\theta_0)\tan\varphi} - r_m,\\
\theta_B &= \arctan\frac{\sin\theta_0}{\cos\theta_0 - A'},\\
\theta_C &= \arctan\frac{\sin\theta_h e^{(\theta_h-\theta_0)\tan\varphi}}{\cos\theta_0 - A' - \left(\sin\theta_h e^{(\theta_h-\theta_0)\tan\varphi} - \sin\theta_0\right)/\tan\beta},\\
A' &= \frac{\sin(\theta_h-\theta_0)}{\sin\theta_h} - \frac{\sin\left(\theta_h+\beta\prime\right)}{\sin\theta_h\sin\beta\prime}\left(e^{(\theta_h-\theta_0)\tan\varphi}\sin\theta_h - \sin\theta_0\right).
\end{aligned} \quad (11)$$

For the slope subjected to pile driving, the external work rate and the energy dissipation rate also include the pile-driving force rate W_p and the lateral forces work rate of piles D_P, respectively.

Following the concept presented by Fan [23], the pile resistance R_T is calculated as follows:

$$R_T = R_s + R_p = \left(0.5 + \frac{z}{100}\right)P_s\frac{\pi d^2}{4} + \pi d\,(0.025P_s + 25)\frac{z}{S_t}, \quad (12)$$

where R_s is the pile side resistance ($R_s = \pi d\,(0.025P_s + 25)\cdot(z/S_t)$) and R_p is the pile tip resistance ($R_p = ((0.5 + (z/100))P_s\pi d^2/4)$). S_t and P_s represent sensitivity of soil and penetration resistance, respectively.

Before the pile passes through the sliding surface, the expression of the pile-driving force power W_P is given as

$$W_P = \omega r_p\cos\theta_p R_T(z). \quad (13)$$

After the pile passes through the sliding surface, only the pile side resistance within the failure surface depth works. The pile-driving force power is then expressed as

$$W_P = \omega r_p \cos\theta_p R_s(h),$$
$$h = r_p \sin\theta_p - r_h \sin\theta_h + X_f \tan\beta. \tag{14}$$

Following the procedure presented by Ito and Matsui [24], the lateral forces acting on a pile can be expressed as

$$p(z) = cD_1\left(\frac{D_1}{D_2}\right)^{N_\varphi^{1/2}\tan\varphi+N_\varphi-1}\left\{\frac{1}{N_\varphi\tan\varphi}\left[\exp\left(\frac{D_1-D_2}{D_2}N_\varphi\tan\varphi\tan\left(\frac{\pi}{8}+\frac{\varphi}{4}\right)\right)-2N_\varphi^{1/2}\tan\varphi-1\right]+\frac{2\tan\varphi+2N_\varphi^{1/2}+N_\varphi^{-(1/2)}}{N_\varphi^{1/2}\tan\varphi+N_\varphi-1}\right\}$$
$$-c\left[D_1\frac{2\tan\varphi+2N_\varphi^{1/2}+N_\varphi^{-(1/2)}}{N_\varphi^{1/2}\tan\varphi+N_\varphi-1}-2D_2N_\varphi^{-(1/2)}\right]+\frac{\gamma z}{N_\varphi}\left[D_1\left(\frac{D_1}{D_2}\right)^{N_\varphi^{1/2}\tan\varphi+N_\varphi-1}\cdot\exp\left(\frac{D_1-D_2}{D_2}N_\varphi\tan\varphi\tan\left(\frac{\pi}{8}+\frac{\varphi}{4}\right)\right)-D_2\right],$$
$$N_\phi = \tan^2\left(\frac{\pi}{4}+\frac{\phi}{2}\right), \tag{15}$$

where D_1 and D_2 are the center-to-center spacing and boundary spacing between piles, respectively. The main purpose of this article is to evaluate the three-dimensional stability of slopes during single pile driving. When calculating the lateral force, the center-to-center spacing in the formula equals B and the boundary spacing between piles in the formula equals $(B-d)$, where B is the finite width of the mechanism and d is the pile diameter. According to Gao et al. [17], for simplicity, the rate of energy dissipation done by the resistance of the piles is calculated as

$$D_p = \omega\int_0^h P(z)l(z)\mathrm{d}z, \tag{16}$$

$$l(z) = r_h\sin\theta_h - X_f\tan\beta + z. \tag{17}$$

2.3. Heterogeneity and Anisotropy of Soil. As mentioned above, the soils are assumed to be homogeneous and isotropic with uniform strength parameters in the majority of existing studies. However, in reality, every mass of natural soil exhibits some anisotropy in the shear direction and some nonhomogeneity in the depth direction, which could significantly affect the shear strength of the soil, thereby leading to the changes in the factor of safety of slope stability. In this paper, the Mohr–Coulomb yield criterion is employed for the slope stability analyses, which includes two parameters: cohesion c and internal friction angle φ. Various scholars concluded that the influence of anisotropy of the internal friction angle on stability of slope can be ignored [25–27]. Meanwhile, it becomes so complex mathematically that the nonhomogeneity of the internal friction angle is taken into consideration in conventional kinematic analysis of slope stability. Qin and Chian [28] have concluded that the influence of linear increasing with depth in the internal friction angle is analogous to cohesion that a larger internal friction angle is of great benefit to the slope stability. Hence, for simplicity, it is assumed that only the cohesive c is nonuniform and anisotropic, and the internal friction angle φ remains uniform and isotropic.

In terms of the geometric relationship illustrated in Figure 3, the cohesion of slope surface can be expressed as

$$c_f = n_0 c, \qquad \theta_0 \le \theta \le \theta_B,$$
$$c_f = c\left[n_0 + \frac{h_f}{H}(1-n_0)\right], \quad \theta_B \le \theta \le \theta_C, \tag{18}$$
$$c_f = c, \qquad \theta_C \le \theta \le \theta_h,$$

where

$$H = r_h\sin\theta_h - r_0\sin\theta_0,$$
$$h_f = r_f\sin\theta - r_0\sin\theta_0, \tag{19}$$

where r_f = the distance between the rotation center O and slope face and H = the height of the slope. The expression of r_f is given as

$$r_f = \frac{r_0 r_h\sin(\theta_h-\theta_0)}{r_0\sin(\theta-\theta_0)-r_h\sin(\theta-\theta_h)}. \tag{20}$$

The cohesion of the 3D spiral structure can be expressed as

$$c = \frac{y-a}{R-a}c_b + \frac{R-y}{R-a}n_0 c, \quad \theta_0 \le \theta \le \theta_B,$$
$$c = \frac{y-d}{R-d}c_b + \frac{R-y}{R-d}\left[n_0 + \frac{h_f}{H}(1-n_0)\right]c, \quad \theta_B \le \theta \le \theta_C,$$
$$c = \frac{y-e}{R-e}c_b + \frac{R-y}{R-e}c, \quad \theta_C \le \theta \le \theta_h,$$
$$c_b = c\left[n_0 + \frac{h_b}{H}(1-n_0)\right],$$
$$h_b = r\sin\theta - r_0\sin\theta_0, \tag{21}$$

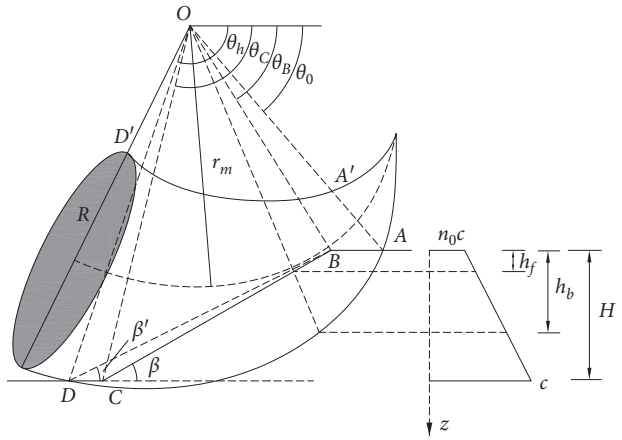

Figure 3: Nonhomogeneous slope.

where c_b = the cohesion of the slide surface and h_b = the distance between slide surface and slope crest. More details are presented in [29]. Following the concept presented by Chen [22], the anisotropy of soil cohesion in the slope can be described as

$$c_i = c_v\left(1 - \frac{1-k}{k}\cos^2 i\right), \tag{22}$$

where $i = \theta + \delta - (\pi/2) - \varphi$, $\delta = (\pi/4) + (\varphi/2)$.

2.4. Factor of Safety. Based on the force-increase technique, the safety factor F_S can be expressed as

$$F_S = \frac{D}{W} = \frac{D_c + D_e + D_p}{W_c + W_e + W_p}. \tag{23}$$

In order to obtain the minimum F_S and the corresponding sliding surface, the parameters describing the shape of slope $(\theta_0, \theta_h, (r_0'/r_0), b, \beta\prime)$ are optimized by MATLAB. The objective function and constraints of the optimization can be expressed as follows:

$$\min f = f\left(\theta_0, \theta_h, (r_0'/r_0), b, \beta\prime\right) \quad \text{s.t.} \begin{cases} 0 < \theta_0 < \pi/2 \\ \theta_0 < \theta_h < \pi \\ 0 < r'/r_0 < 1 \\ 0 < b < B \\ 0 < \beta\prime < \beta \end{cases}. \tag{24}$$

3. Validation

In order to verify the effectiveness and accuracy of the proposed method, the F_S is compared with that calculated by Gao et al. [17] and Yang and Li [18]. Noted that, for comparison, the same values of parameters used in the literature were also used in this paper. Without consideration of piles driving, it is found that the results obtained from the proposed method and the approach by Yang and Li [18] are in a very good agreement as presented in Table 1.

Table 1: Comparisons of the factor of safety ($H = 20, \gamma = 19, c = 38, \varphi = 20^\circ, \beta = 45^\circ$).

B/H	2	5	10	2D
F_S [18]	1.9556	1.7405	1.6771	1.6177
F_S (in this paper)	1.9544	1.7402	1.6769	1.6177

Taking piles driving into consideration, the F_S obtained in this paper is compared with that calculated by Gao et al. [17]. It can be seen from Table 2 that the F_S calculated by two methods has qualitative agreement with each other, which verifies the effectiveness and accuracy of the method proposed in this paper. Meanwhile, the F_S obtained in this paper is smaller. Reasons are as follows: (i) Gao et al. [17] considered the effect of group piles on the stability of a slope while the effect of single pile driving on the stability of a slope is discussed in this paper; (ii) from the perspective of mathematics, the rate of dissipation for piles is simplified. The dissipation rate of two end parts is omitted; (iii) the work rate done by single pile driving is considered through adding an additional item into external work rate.

4. Parametric Study

4.1. Anisotropic and Nonhomogeneous Coefficient. Figure 4 shows the effect of anisotropic coefficient k on the F_S during the pile-driving process. The parameters used in the calculations are as follows: unit weight $\gamma = 19\,\text{kN/m}^3$, soil cohesion $c = 30\,\text{kPa}$, internal friction angle $\varphi = 20^\circ$, slope angle $\beta = 45^\circ$, nonhomogeneity coefficient $n_0 = 1$, the ratio $(B/H) = 1$, pile location $(X_f/L_X) = 0.7$, pile width $d = 1.5\,\text{m}$, sensitivity of soil $S_t = 1.6$, and penetration resistance $P_s = 1.2\,\text{MPa}$. To investigate the effect of anisotropy of soil, various values of k are used. It is observed that throughout the pile-driving process, the F_S decreases significantly with decreasing values of k, which indicates that the anisotropic property of soil has an unfavorable effect on the stability of the slope during pile driving. As seen from Figure 4, when $k = 0.7$, the values of F_S are much smaller than those are when $k = 1$, and the slope tends to collapse. Similarly, to characterize different extents of nonhomogeneity, various values of n_0 are used in Figure 5. It can be found that during the whole process of pile driving, the F_S of the slope decreases substantially as the nonhomogeneous coefficient decreases from 1 to 0.7. As shown in Figure 5, the values of F_S corresponding to $n_0 = 0.7$ are much smaller than those corresponding to $n_0 = 1$. Therefore, it is of great theoretical value to consider the anisotropy and heterogeneity of soil.

4.2. Soil Cohesion and Internal Friction Angle. Figures 6 and 7 present the effect of cohesion c and internal friction angle φ on slope stability considering the pile-driving process. As shown in Figure 6, a substantial increase in the F_S can be observed with increasing value of c, but the overall trend of each curve follows the similar pattern. It can be seen from Figure 7 that the internal friction angle of soil largely influences the F_S, especially when the friction angle is relatively

Table 2: Comparisons of the factor of safety ($H = 10, \gamma = 19.63, c = 23.94, \varphi = 10^{\circ}, \beta = 45^{\circ}$, $(B/H) = 2$).

X_f/L_X	0.3	0.4	0.5	0.6
F_S [17]	1.487	1.582	1.680	1.762
F_S (in this paper)	1.455	1.478	1.502	1.512

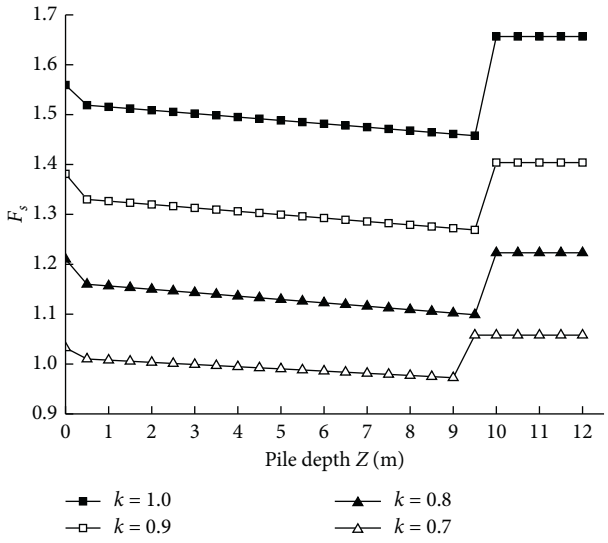

Figure 4: Effects of the anisotropy coefficient on the stability of 3D slopes.

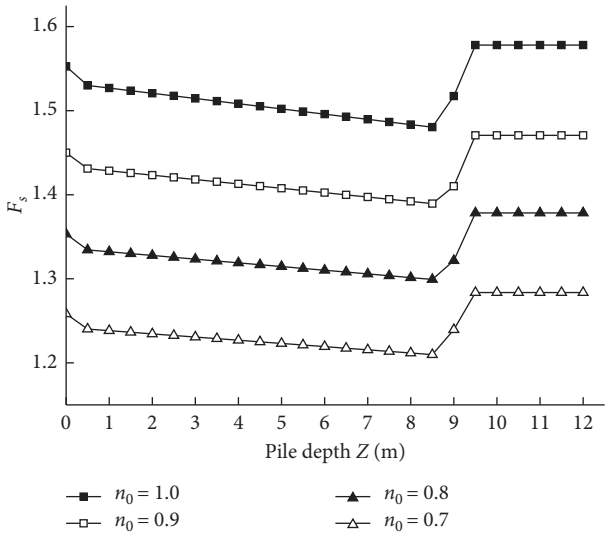

Figure 5: Effects of the nonhomogeneous coefficient on the stability of 3D slopes.

high (e.g., $\varphi = 20^{\circ}$ and 25°), but the change rule of the F_S during pile driving remains unchanged for various angles. In addition, $\beta\prime$ is always equal to β throughout the pile-driving process, which indicates that the toe failure occurs. This is consistent with the description of Chen [22].

4.3. The Inclined Angle. Figure 8 illustrates the effect of various values of inclined angle β on assessment of slope

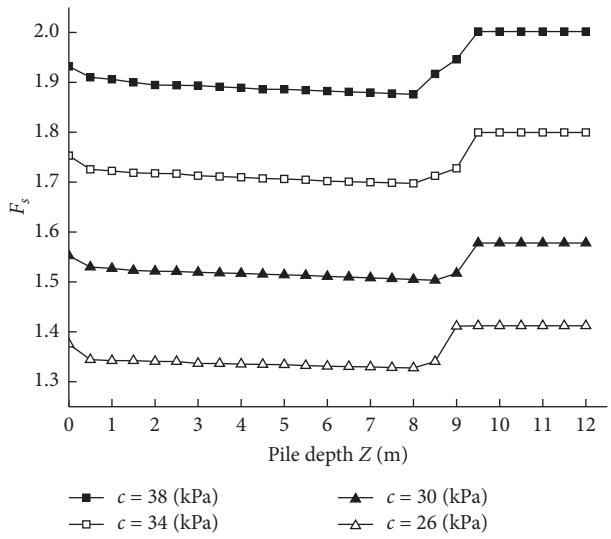

Figure 6: Effects of soil cohesion on the stability of 3D slopes.

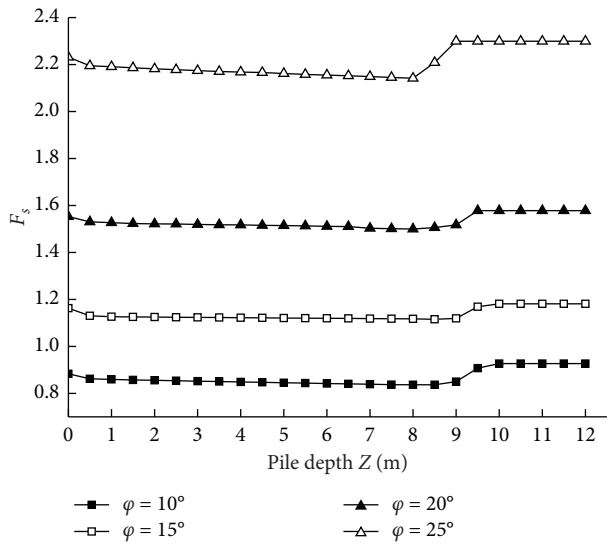

Figure 7: Effects of the friction angle of soil on the stability of 3D slopes.

stability during the pile-driving process. Nonhomogeneity and anisotropy are still in consideration ($n_0 = 0.7$ and $k = 0.9$). As described in Figure 8, with the increase of β, the values of F_S decrease rapidly, especially when the inclined angle is changing from 25° to 45°. For steep slopes, the inclined angle of a slope has a significant influence on the factor of safety of a slope, which means the effect of pile driving on slope stability cannot be neglected. For gentle slopes, the process of single pile driving has little effect on the F_S.

4.4. The Ratio (B/H). As shown in Figure 9, the change of the F_S is sensitive to the change of ratio (B/H), especially when the ratio of (B/H) is relatively small (e.g., $(B/H) = 1, 2$, and 5). The values of F_S decrease significantly as ratio (B/H) increases from value 1 to 10. Figure 9 shows that as the ratio

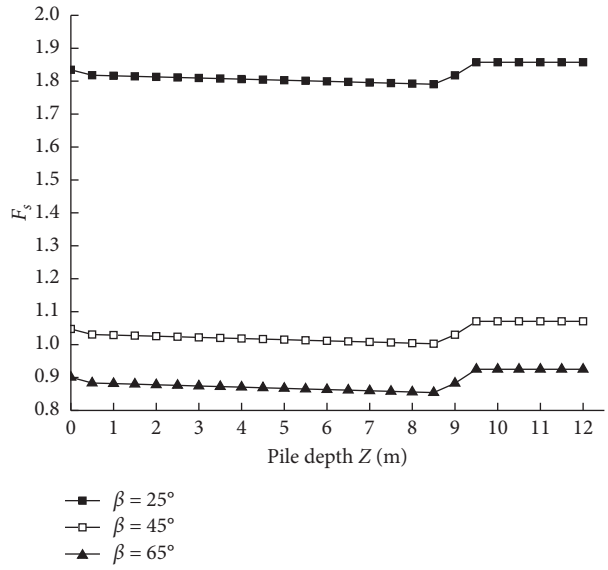

Figure 8: Effects of the inclined angle of soil on the stability of 3D slopes.

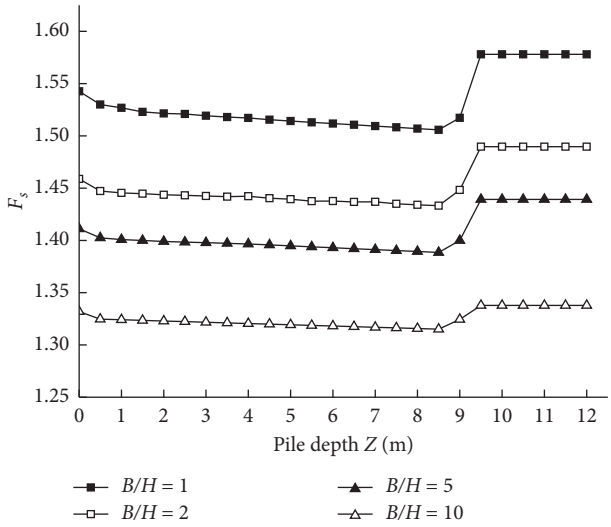

Figure 9: Effects of the B/H ratio on the stability of 3D slopes.

(B/H) increases, the values of F_S decrease significantly. When the slope is constrained in a narrower width, the slope is more stable, which means the three-dimensional effect of the slope cannot be ignored. To be specific, the failure mechanism consists of the three-dimensional spiral parts and the plane insert part. The gravity work rate of 3D spiral parts is smaller than the plane insert part with a same width, and the energy dissipation work rate of 3D spiral parts is greater. While the width of 3D spiral parts is relatively stable, the increase of the slope width results in a decrease in the ratio of internal work rate to external work rate, and the factor of safety of a slope decreases.

4.5. Pile Location. Figure 10 describes the effect of various values of the ratio (X_f/L_X) on the F_S during pile driving. Figure 10 also shows that the position of the pile has great

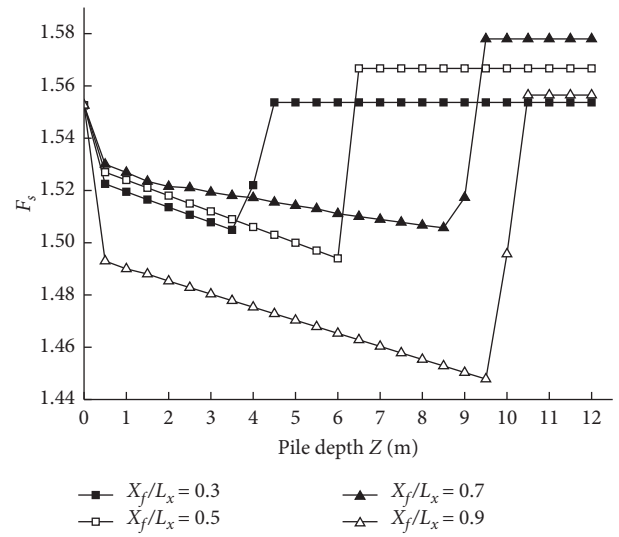

Figure 10: Effects of pile location X_f/L_X on the stability of 3D slopes.

influences on the F_S. The closer the pile position is to the bottom of the slope, the smaller the reduction in the F_S is and the earlier the F_S reaches the maximum. The reason is that when the pile is near the bottom of the slope, the pile can pass through the sliding surface earlier, and then the F_S reaches the maximum and becomes stable. When the pile is near the top of the slope, the vertical distance of the sliding surface to the slope reaches the maximum. Before the pile reaches the sliding surface, as the depth of the pile increases, the F_S continues to decrease and finally reaches the minimum value, and the time required for the pile to reach the sliding surface is longer. For the overall consideration, the optimum location for pile sinking is about $(X_f/L_X) = 0.7$. Due to that, at this location, the reduction of F_S at the initial stage of pile sinking is relatively small, and the reinforcement effect of the pile is high.

The reason for the best reinforcement effect at $(X_f/L_X) = 0.7$ can be explained as follows: when the pile is near the bottom of the slope, the force arm is large, but the lateral force distribution range is small, and when the pile is near the top of the slope, the force arm is small, but the lateral force distribution range is large. According to formula (16), when $(X_f/L_X) = 0.7$, the work rate of lateral force between piles is the largest, which means the pile reinforcement effect is the best.

4.6. Summary. Figures 4–10 show that, at the initial state of the pile-driving process when the pile body is jacked into the soil, the F_S is reduced suddenly. Since the pile starts to sink into the soil, the equivalent pile tip resistance and equivalent pile side resistance begin to work and the external work rate W_P increases, which subsequently leads to a decrease in the F_S. In contrast, after the pile passes through the sliding surface, the F_S tends to rise dramatically, thereafter it remains stable. It is because the pile is passing through the sliding surface that the equivalent pile tip resistance does not

work and the lateral force of the pile begins to work, which subsequently leads to an increase in the F_S.

5. Conclusions

This article presents a new method to estimate the factor of safety (F_S) of slopes during pile driving based on the 3D horn mechanism. By employing the upper-bound theorem and force-increase technique, the explicit expression of the F_S is obtained. The lowest solution among all possible results is sought by an optimization program developed in MATLAB. The effectiveness and accuracy of the proposed method is well demonstrated by comparing the results obtained from the proposed approach and the solutions from published literatures. In particular, the anisotropy and heterogeneity of soil have been taken into account in the analysis.

The estimation of the F_S is very important for the stability analysis of the slope during pile driving. The values of the F_S depend on the soil properties, the geometries of 3D slopes, and pile location. The results of this study indicate that, the anisotropy and heterogeneity of soil have adverse effect on slope stability; for steep slopes, the effect of pile driving cannot be neglected in assessment of the stability of slopes. In the process of pile driving, the F_S decreases significantly until the pile tip reaches the failure surface of the slope, while the F_S increases dramatically after the pile passes through the failure surface, thereby revealing the pile reinforcement effect. The optimal pile location is found to be at $(X_f/L_X) = 0.7$. These observations highlight that the adverse effects of the pile-driving process should be highly concerned during the design of geotechnical infrastructures, rather than emphasizing the reinforcement effect of a pile only.

Data Availability

The data used to support the findings of this study are included within the article.

Conflicts of Interest

The authors declare that there are no conflicts of interest.

Acknowledgments

The research presented in this paper was supported financially by the first author, Pingping Rao. The authors sincerely thank the kind assistance provided by Yunwei Shi.

References

[1] R. L. Michalowski and A. Drescher, "Three-dimensional stability of slopes and excavations," *Géotechnique*, vol. 59, no. 10, pp. 839–850, 2009.

[2] H. J. Hovland, "Three-dimensional slope stability analysis method," *Journal of the Geotechnical Engineering Division*, vol. 103, no. 9, pp. 971–986, 1977.

[3] A. S. Azzouz and M. M. Baligh, "Loaded areas on cohesive slopes," *Journal of Geotechnical Engineering*, vol. 109, no. 5, pp. 724–729, 1983.

[4] L. Lam and D. G. Fredlund, "A general limit equilibrium model for three-dimensional slope stability analysis," *Canadian Geotechnical Journal*, vol. 30, no. 6, pp. 905–919, 1993.

[5] W. B. Wei, Y. M. Cheng, and L. Li, "Three-dimensional slope failure analysis by the strength reduction and limit equilibrium methods," *Computers and Geotechnics*, vol. 36, no. 1-2, pp. 70–80, 2009.

[6] F. Cai and K. Ugai, "Numerical analysis of the stability of a slope reinforced with piles," *Soils and Foundations*, vol. 40, no. 1, pp. 73–84, 2000.

[7] J. Won, K. You, S. Jeong, and S. Kim, "Coupled effects in stability analysis of pile-slope systems," *Computers and Geotechnics*, vol. 32, no. 4, pp. 304–315, 2005.

[8] D. V. Griffiths and R. M. Marquez, "Three-dimensional slope stability analysis by elasto-plastic finite elements," *Géotechnique*, vol. 57, no. 6, pp. 537–546, 2007.

[9] T.-K. Nian, R.-Q. Huang, S.-S. Wan, and G.-Q. Chen, "Three-dimensional strength-reduction finite element analysis of slopes: geometric effects," *Canadian Geotechnical Journal*, vol. 49, no. 5, pp. 574–588, 2012.

[10] H. Shen and S. M. Abbas, "Rock slope reliability analysis based on distinct element method and random set theory," *International Journal of Rock Mechanics and Mining Sciences*, vol. 61, pp. 15–22, 2013.

[11] Z. Chen, X. Wang, C. Haberfield, J.-H. Yin, and Y. Wang, "A three-dimensional slope stability analysis method using the upper bound theorem: part I: theory and methods," *International Journal of Rock Mechanics and Mining Sciences*, vol. 38, no. 3, pp. 369–378, 2001.

[12] E. Ausilio, E. Conte, and G. Dente, "Stability analysis of slopes reinforced with piles," *Computers and Geotechnics*, vol. 28, no. 8, pp. 591–611, 2001.

[13] J. S. Xu, Y. Li, and X. L. Yang, "Stability charts and reinforcement with piles in 3D nonhomogeneous and anisotropic soil slope," *Geomechanics and Engineering*, vol. 14, no. 7, pp. 71–81, 2018.

[14] J. S. Xu, Q. J. Pan, X. L. Yang, and W. T. Li, "Stability charts for rock slopes subjected to water drawdown based on the modified nonlinear Hoek-Brown failure criterion," *International Journal of Geomechanics*, vol. 18, no. 1, Article ID 04017133, 2018.

[15] L. C. Reese, "Analysis of laterally loaded piles in weak rock," *Journal of Geotechnical and Geoenvironmental Engineering*, vol. 123, no. 11, pp. 1010–1017, 1997.

[16] E. Conte, A. Troncone, and M. Vena, "Behaviour of flexible piles subjected to inclined loads," *Computers and Geotechnics*, vol. 69, pp. 199–209, 2015.

[17] Y.-f. Gao, M. Ye, and F. Zhang, "Three-dimensional analysis of slopes reinforced with piles," *Journal of Central South University*, vol. 22, no. 6, pp. 2322–2327, 2015.

[18] X. L. Yang and Z. W. Li, "Factor of safety of three-dimensional stepped slope," *International Journal of Geomechanics*, vol. 18, 2018.

[19] C. Sun, J. Chai, Z. Xu, and Y. Qin, "3D stability charts for convex and concave slopes in plan view with homogeneous soil based on the strength-reduction method," *International Journal of Geomechanics*, vol. 17, no. 5, Article ID 06016034, 2017.

[20] C. C. Swan and K. S. Young, "Limit state analysis of earthen slopes using dual continuum/FEM approaches," *International Journal for Numerical and Analytical Methods in Geomechanics*, vol. 23, no. 12, pp. 1359–1371, 1999.

[21] L. C. Li, C. A. Tang, W. C. Zhu, and Z. Z. Liang, "Numerical analysis of slope stability based on the gravity increase

method," *Computers and Geotechnics*, vol. 36, no. 7, pp. 1246–1258, 2009.
[22] W. F. Chen, *Limit Analysis and Soil Plasticity*, Elsevier, Amsterdam, Netherlands, 1975.
[23] X. Y. Fan, *Study of Sinking-Resistance and Compaction Effect of Static-Press Pile*, Tongji University, Shanghai, China, 2007.
[24] T. Ito and T. Matsui, "Methods to estimate lateral force acting on stabilizing piles," *Soils and Foundations*, vol. 15, no. 4, pp. 43–59, 1975.
[25] J. M. Duncan and H. B. Seed, "Anisotropy and stress reorientation in clay," *Journal of the Soil Mechanics and Foundation Division, ASCE*, vol. 92, pp. 21–50, 1966.
[26] P. W. Mayne, "Stress anisotropy effects on clay strength," *Journal of Geotechnical Engineering, ASCE*, vol. 111, pp. 326–366, 1985.
[27] A. A. AI-Karni and M. A. AI-Shamrani, "Study of the effect of soil anisotropy on slope stability using method of slices," *Computers and Electronics in Agriculture*, vol. 26, no. 2, pp. 83–103, 2000.
[28] C.-B. Qin and S. C. Chian, "Kinematic analysis of seismic slope stability with a discretisation technique and pseudo-dynamic approach: a new perspective," *Géotechnique*, vol. 68, no. 6, pp. 492–503, 2018.
[29] J. P. Li, "Upper-bound limit analysis on stability of three-dimensional slopes considering soil nonhomogeneity," *Journal of Tongji University (Natural Science)*, vol. 45, no. 10, pp. 46–51, 2018, in Chinese.